pubs.acs.org/Biomac

Article

Enzymatically Active DNA-Protein Nanogels with Tunable Cross-Linking Density

Marina Mariconti, Mathieu Morel, Damien Baigl, and Sergii Rudiuk*

Cite This: *Biomacromolecules* 2021, 22, 3431−3439

Read Online

ACCESS | Metrics & More | Article Recommendations | Supporting Information

ABSTRACT: Hybrid DNA-protein nanogels represent potential protein vectors and enzymatic nanoreactors for modern biotechnology. Here, we describe a new, easy, and robust method for preparation of tunable DNA-protein nanogels with controllable size and density. For this purpose, polymerase chain reaction is used to prepare highly biotinylated DNA as a soft biopolymeric backbone, which can be efficiently cross-linked via streptavidin-biotin binding. This approach enables us to control both the density and size of the resulting nanogels not only by adjusting the amount of the cross-linking streptavidin but also by using different rates of DNA biotinylation. This gives DNA-streptavidin nanogels with the size ranging from 80 nm, for the most compact state, to up to 200 nm. Furthermore, using streptavidin-enzyme conjugates allows the straightforward one-pot incorporation of enzymes during the preparation of the nanogels. Monoenzymatic and multienzymatic nanogels have been obtained in this manner, and their catalytic activities have been characterized. All tested enzymes (alkaline phosphatase (AP), horseradish peroxidase (HRP), and β-galactosidase (βGal)), incorporated individually or in a coupled manner (glucose oxidase (GOx)-HRP cascade), were shown to remain functional. The activities of AP and βGal were unchanged while that of HRP was slightly improved inside the nanogels. We demonstrate that, for HRP, it is not the DNA-to-enzyme ratio but the physical density of the functionalized DNA nanogels that is responsible for the improvement of its enzymatic activity.

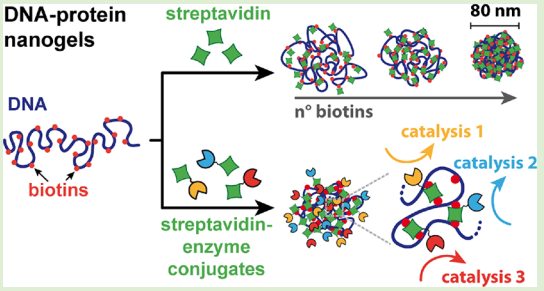

1. INTRODUCTION

Besides encoding genetic information, DNA combines a series of properties that make it a particularly versatile and useful material.[1] Highly charged and semi-flexible, DNA is a water-soluble and biocompatible polyelectrolyte. Not only can it be biosourced, but it also offers the possibility to be synthesized of virtually any size and sequence. Finally, unique programmability of DNA through sequence-specific base pairing enables the controlled assembly and functionality of various DNA nanostructures.[2−4] As a consequence, a number of DNA-based materials have been extensively described in the literature, such as organized DNA structures (e.g., DNA origamis,[5,6] nanostructures made from DNA tiles or bricks,[7,8] DNA nanogrids,[4] etc.) or more disordered structures (e.g., DNA-grafted polymers or DNA-based hydrogels).[9,10] Recently, DNA nanogels (DNA NGs) emerged in this field due to the possibility of combining a dense 3D nanogel network[11,12] with specific properties of DNA, resulting in a new class of biomaterials promising for biomedical applications such as gene and drug delivery.[13] To broaden their applications, DNA NGs have been further functionalized, with various entities such as siRNAs for gene delivery,[14,15] aptamers for specific binding to biomarkers,[16] or biologically active substances for drug delivery.[17] Although enzymes and other proteins can be incorporated into DNA nanostructures,[18] up to now, there is only one reported example of DNA NGs containing proteins,[19] and to the best of our knowledge, DNA NGs carrying active enzymes have never been described in the literature.

Here, we propose a new method for the preparation of DNA NGs having the advantage to be easily functionalizable with a large number of active proteins and, in particular, enzymes. Our strategy is based on the cross-linking of a multi-biotinylated DNA backbone with streptavidin proteins. This approach has been recently explored to induce cross-linking within a giant DNA scaffold biotinylated by photochemical binding of apsoralene-biotin conjugate, but because of the low biotinylation efficiency, the resulting micrometer-size objects had a loose density.[20] To obtain nanosized and dense DNA-streptavidin gels, the use of short and highly biotinylated DNA scaffolds was thus required. Here, the preparation of such scaffolds was achieved by polymerase chain reaction (PCR), an enzymatic technique consisting of DNA amplification through multiple consecutive steps of denaturation and replication of selected DNA fragments by DNA polymerase in the presence

Received: April 19, 2021
Revised: June 25, 2021
Published: July 14, 2021

https://doi.org/10.1021/acs.biomac.1c00501
Biomacromolecules 2021, 22, 3431−3439

of a mixture of deoxynucleotide triphosphates (dNTPs).[21] A largely used tool in molecular biology, PCR for instance found applications for quantification of nucleic acids (quantitative PCR and digital PCR),[22,23] reporting of proteins in the ELISA technique (immuno-PCR),[24] genotyping (amplification-refractory mutation system PCR),[25] and even introducing covalent modifications in the DNA duplex, for instance, biotin residues,[26,27] but has not been explored much for the preparation of DNA-based materials.

We thus developed new hybrid DNA-based nanobiomaterials by combining highly efficient DNA biotinylation via PCR with specific streptavidin-biotin binding,[28] explored the functionalization of the resulting DNA-streptavidin nanogels either with individual enzymes or with a mixture of different enzymes, and evaluated the activities of the incorporated enzymes for different cross-linking densities of DNA nanogels.

2. MATERIALS AND METHODS

2.1. Materials. Biotinylated primers, streptavidin, D-(+)-glucose, isopropanol, and DMSO were purchased from Merck Sigma-Aldrich. Biotin-16-dCTP and dNTP nucleotides were from Jena Bioscience. Q5 polymerase, a gel loading dye, and nuclease digestion mix were from NEB. Streptavidin conjugated with alkaline-phosphatase (AP), horseradish peroxidase (HRP), and β-galactosidase (βGal) together with the corresponding substrates (DDAO phosphate (DDAO-P), an Amplex UltraRed reagent, and DDAO-galactoside (DDAO-G) was from Invitrogen. A streptavidin Alexa Fluor 555 conjugate and FluoReporter Biotin quantitation assay kit were from Invitrogen. Deionized MQ water (18 MΩ·cm) was from Millipore, and nuclease-free water (Ambion) was from Invitrogen. Midori Green Advance DNA stain was from Dutscher. A Qiaquick gel extraction kit was from Qiagen. Streptavidin conjugated with glucose oxidase (GOx) was from MyBioSource.

2.2. Preparation of Multibiotinylated DNA (bt-DNA) by PCR. DNA fragments (3480 bp) were amplified from a plasmid template (T7-ubiD-YFP) by PCR in the presence of 5′-biotinylated forward (5′-[bt]AGGGCGACACGGAAATGTTG) and reverse (5′-[bt]-AGCTTGGAGCGAACGACCTA) primers. Reaction solutions (20 μL) were assembled on ice with the following final composition: 50 μM of each dNTP, 50 ng of the DNA template, 0.5 μM of each primer, 8% (v/v) DMSO, and 0.2 μL of 2000 U/mL Q5 DNA polymerase in 1× Q5 buffer (New England BioLabs Inc.). Biotin-16-dCTP (bt-dCTP) was added to the PCR mixture by substituting 50, 25, 5, or 0% of the non-biotinylated dCTP in the PCR mixture. Then, after the first step at 98 °C for 30 s, 30 cycles (98 °C for 10 s, 60 °C for 20 s, and 72 °C for 3 min) were performed followed by the last step at 72 °C for 5 min. The purity of amplified DNA was checked by depositing 20 μL of the PCR sample with 4 μL of a 6× gel loading dye into 1% agarose gel with 2.5 μL of Midori Green Advance, and the gel was run in a BioRad electrophoresis device (Figure S1). For simplicity, the resulting DNA fragments were named according to the initial composition of the PCR reaction mixture: 50%bt-DNA, 25%bt-DNA, 5%bt-DNA, and 0%bt-DNA. Corresponding bt-DNA bands were then cut out from agarose gel, purified with a Qiaquick gel extraction kit, and resuspended in nuclease-free water. The concentrations of the resulting DNA fragments were determined by absorption using a BioPhotometer plus spectrophotometer (Eppendorf).

2.3. Biotin Quantitation in bt-DNA. *2.3.1. Digestion.* Before detecting biotin concentrations by the HABA assay, the DNA sample was first digested with DNA nuclease in order to separate all biotinylated residues. The digestion was performed in triplicate for 1 h at 37 °C by a 1X nucleoside digestion mix (New England BioLabs Inc.) in 1X NaAc-$ZnCl_2$ buffer. The final DNA concentrations for digestion were adjusted for each bt-DNA to contain approximately the same amount of biotin, i.e., 13.2, 45.2, and 127.6 μM in phosphates for 50%bt-DNA, 25%bt-DNA, and 5%bt-DNA, respectively.

2.3.2. FluoReporter Biotin Quantitation Assay. The FluoReporter assay is based on the displacement of a quenching ligand from the biotin binding sites on fluorescent streptavidine. The decrease in fluorescence quenching can thus be followed by fluorescence spectroscopy. To prepare the calibration curve, increasing concentrations of bt-dCTP were prepared in 1X NaAc-$ZnCl_2$ buffer (0, 0.2, 0.4, 0.6, 0.8, 1.0, 1.2, and 1.6 μM). Each digested bt-DNA sample (25 μL) and the calibration bt-dCTP solutions were loaded in a 96-well plate, and 25 μL of a FluoReport Green reagent was added. Samples were then incubated for 5 min at RT protected from light, and fluorescence was measured with a QuantStudio 5 Real-Time PCR machine (Thermofisher) at λ_{ex} = 470 nm and λ_{em} = 520 nm. All the samples as well as calibration solutions were triplicated, and the average values were then used for data analysis. The calibration curve obtained for different bt-dCTP solutions was fitted (from 0 to 0.4 μM final bt-dCTP concentration) with the power allometric2 equation in Origin software ($y = a + b[\text{biotin}]^c$), and the obtained equation was then used to determine biotin concentrations in the digested bt-DNA samples from their average fluorescence intensity. The biotin quantification assay was triplicated for three different PCR biotinylation reactions.

2.4. Preparation of DNA-Streptavidin Nanogels. In a typical experiment, bt-DNA (at a final concentration of 1 μM in phosphates) was mixed on ice with increasing concentrations of streptavidin (from 0 to 100 nM) in 10 mM Tris/HCl buffer (pH 7.4) prepared in nuclease-free water. We used a 52.8 kDa molecular mass of streptavidin to calculate its molar concentrations. The solutions were then incubated on ice for 1 h to allow the formation of nanogels prior to further investigations or observations.

2.5. Monoenzyme-Functionalized DNA Nanogels. *2.5.1. Preparation.* Functionalized DNA nanogels were prepared at a 1 μM final phosphate concentration of 50%bt-DNA in 10 mM Tris/HCl buffer (pH 7.4) in the presence of 10 nM streptavidin-enzyme conjugates for streptavidin-HRP (sHRP, M_w = 96.8 kDa) or streptavidin-AP (sAP, M_w = 192.8 kDa) and 1 nM streptavidin-β-galactosidase (sβGal, M_w = 572.8 kDa) in the presence of 19 nM streptavidin at a final volume of 50 μL. For control experiments, the streptavidin-enzyme conjugates were mixed in the same conditions with non-biotinylated 0%bt-DNA (1 μM in phosphates) or with 10 mM Tris/HCl buffer. For sβGal, an additional control without streptavidin was performed. All these solutions were prepared in triplicate. All samples were then incubated on ice for 2 h to allow the formation of enzyme-functionalized nanogels. Molecular weights of streptavidin-enzyme conjugates were considered as the sum of the molecular weights of streptavidin (52.8 kDa) and individual enzymes (44, 140, and 520 kDa).

2.5.2. Enzymatic Activity Measurements. After formation of the nanogels, they were diluted with 10 mM Tris/HCl buffer to a 0.5 nM final concentration of streptavidin-enzyme conjugates and incubated at different temperatures (0 °C (on ice), 25 °C, 37 °C, or 50 °C) for 1 h. Then, 50 μL of each sample (in triplicate) was loaded into a 96 black well plate and 50 μL of Amplex UltraRed, 50 μL of the 20 μM DDAO-P substrate, or 50 μL of 150 μM DDAO-G was, respectively, added to sHRP, sAP, or sβGal samples to reach 0.25 nM final enzyme concentrations in each well. Enzymatic reactions were then monitored by fluorescence at 30 °C for 1.5 h with a plate reader (BioTek) with λ_{ex} = 530 nm and λ_{em} = 590 nm for sHRP and λ_{ex} = 590 nm and λ_{em} = 645 nm for both sAP and sβGal. The efficiency of enzymatic reactions was measured as the initial slopes of fluorescence versus time. As reference of the enzymatic activity, fresh sHRP, sAP, or sβGal enzymes were used. They were unfrozen and diluted to 0.5 nM in 10 mM Tris/HCl buffer right before adding substrates into all sample and control mixtures. The initial fluorescence slopes for these reference samples were taken as 100% enzymatic activity.

2.6. Effect of Nanogels Densities on HRP Activity. *2.6.1. Fixed Enzyme Concentration.* A fixed concentration of sHRP (20 nM final concentration) was mixed in triplicate with 1 μM (in phospates) of different biotinylated DNA (50%bt-DNA, 25%bt-DNA, or 5%bt-DNA) in 10 mM Tris/HCl buffer. In control experiments, non-biotinylated 0%bt-DNA or 10 mM Tris/HCl buffer alone was used instead of bt-DNA.

https://doi.org/10.1021/acs.biomac.1c00501
Biomacromolecules 2021, 22, 3431−3439

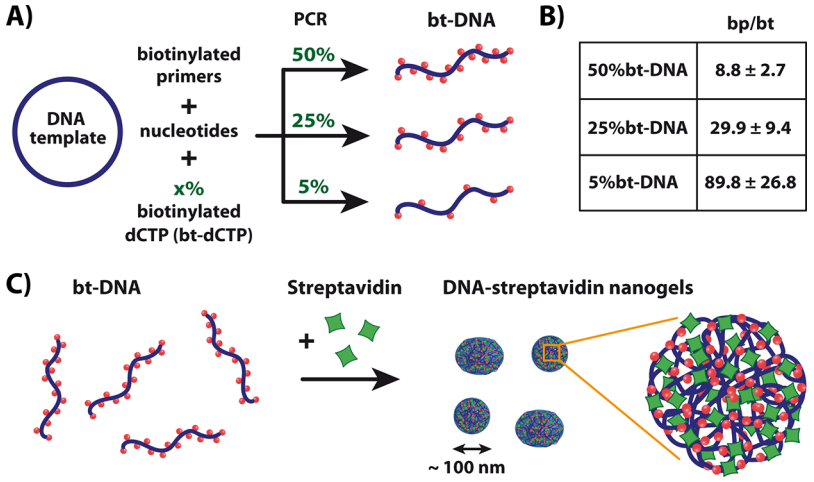

Figure 1. Preparation of DNA-streptavidin nanogels. (A) Scheme of preparation of the multibiotinylated 3480 bp DNA scaffold (bt-DNA) by PCR reaction in the presence of varied amounts (50, 25, or 5%) of biotinylated dCTP (bt-dCTP); %bt-dCTP = [bt-dCTP]/([bt-dCTP] + [dCTP]). (B) Measured DNA biotinylation by PCR in the presence of 50, 25, or 5% of bt-dCTP expressed as the number of base pairs per one biotin residue actually incorparated in the backbone (bp/bt). (C) Adding streptavidin to the resulting bt-DNA induces folding into nanogel structures through multiple cross-linking via streptavidin-biotin interactions.

2.6.2. Fixed Enzyme/Biotin Ratio. To keep the ratio of streptavidin-enzyme conjugates to biotin residues on bt-DNA, the final concentration of sHRP was adjusted for each bt-DNA. The nanogels were formed from 1 μM final phosphate concentrations of 50%bt-DNA, 25%bt-DNA, and 5%bt-DNA in 10 mM Tris/HCl buffer in the presence of 20, 13, and 2 nM sHRP, respectively. The corresponding controls (sHRP in the presence of non-biotinylated DNA and sHRP alone) were also prepared for each enzyme concentration.

All samples were then incubated on ice for 2 h and diluted with 10 mM Tris/HCl, and the activity of the HRP enzyme was measured as previously mentioned at a final sHRP concentration of 0.25 nM.

2.7. Multienzyme-Functionalized Nanogels. *2.7.1. Preparation.* Multienzyme-NGs were prepared by adding a mixture of sHRP, sAP, and sβGal (9.5, 9.5, and 1 nM final concentrations, respectively) to 50%bt-DNA (1 μM final concentration in phosphates) in 10 mM Tris/HCl buffer (pH 7.4) for a final volume of 50 μL. For control experiments in the absence of DNA, the streptavidin-enzyme conjugates were mixed in the same conditions with 10 mM Tris/HCl buffer. Samples were incubated on ice for 1 h to allow the formation of nanogels. All solutions were prepared in triplicate.

2.7.2. Enzymatic Activity Measurements. The enzymatic activity assays were measured separately for each of the three enzymes. Multienzyme-NGs were diluted with 10 mM Tris/HCl buffer to a 0.5 nM final concentration of the tested enzyme. Then, 50 μL of each sample (in triplicate) was loaded into a 96 black well plate and 50 μL of Amplex UltraRed, 50 μL of the 20 μM DDAO-P substrate, or 50 μL of 150 μM DDAO-G was, respectively, added to multienzyme-NGs to assay the enzymatic activities of sHRP, sAP, or sβGal to reach 0.25 nM final enzyme concentrations for the tested enzyme. Enzymatic reactions were monitored by fluorescence at 30 °C for 1 h with a plate reader (BioTek) with λ_{ex} = 530 nm and λ_{em} = 590 nm for sHRP and λ_{ex} = 590 nm and λ_{em} = 645 nm for both sAP and sβGal. The efficiency of enzymatic reactions was measured as the initial slopes of fluorescence versus time. As reference of the enzymatic activity, a fresh mixture of sHRP, sAP, or sβGal enzymes was used. The enzyme-streptavidin conjugates were unfrozen and diluted to 0.5 nM in 10 mM Tris/HCl buffer right before adding substrates into all sample and control mixtures. The initial fluorescence slopes for the reference samples were taken as 100% enzymatic activity.

2.8. Atomic Force Microscopy (AFM). Freshly cleaved mica slides (potassium aluminosilicate (Muscovite Mica) from Goodfellow) were treated for 3 min with 30 μL of 1 mM spermine solution in MQ water, and the excess spermine was removed by by thoroughly rinsing with MQ water. The sample (50 μL) was then deposited on the treated mica, and nanogels were let to adsorb for 1 h in a wet atmosphere at room temperature. After adsorption, the mica slides were washed again with MQ water and dried under the jet of compressed air. AFM measurements were performed on the dried samples using a 5100 atomic force microscope (Agilent Technologies-Molecular Imaging) or Cypher ES atomic force microscope (Oxford Instruments) in tapping mode using a silicon cantilever (Applied NanoStructures-FORT) with a resonance frequency of 43−81 kHz and a Spring constant of 0.6−3.7 N/m.

2.9. ζ-Potential Measurements. Nanogels were prepared at a 1 μM final phosphate concentration of 50%bt-DNA in 10 mM Tris/HCl buffer (pH 7.4) in the presence of increasing concentrations of streptavidin ([strep] = 0, 25, 50, 75, and 100 nM) and incubated on ice for 1 h. The ζ-potential was then measured for these solutions in triplicate with Zetasizer Nano-ZS (Malvern Instruments) at 25 °C. As control, the ζ-potential of free streptavidin was measured at [strep] = 1 μM. An aliquot of each sample was kept for AFM imaging in air. Freshly cleaved mica slides were treated with 1 mM poly-L-lysine (PLL) for 3 min, and the nanogel samples were let to adsorb before being rinsed and dried with compressed air. They were then imaged with a 5100 atomic force microscope (Agilent Technologies, Molecular Imaging) in air.

2.10. Height Profile Analysis of Nanogels at Optimal Streptavidin Concentration. The heights of the nanogels formed from 50%bt-DNA, 25%bt-DNA, and 5%bt-DNA at [strep] = 25, 15, and 5 nM, respectively, were analyzed in two different ways. (A) The average maximum height was calculated using Gwyddion software. Grain analysis was performed on one 2 × 2 μm^2 AFM image for each sample. The height threshold was adjusted to select the nanogel particles, and resulting objects were filtered by area and edge-touching options. The average maximum height (Max Z) and root mean square deviation (RMS) were then calculated for the selected nanogel particles. (B) The 3D profiles of the nanogels were obtained on Cypher software from 2 × 2 μm^2 AFM images (Figure S7).

2.11. Frequency Distribution of Feret Diameter. Typically, the frequency distribution of Feret diameters of individual objects detected on two AFM 5 × 5 μm^2 images for each condition was obtained either by manual measurement of the longest distance between two opposite points within the same object or by automated analysis with Fiji ImageJ software. At least 200 objects per sample were analyzed. For Fiji analysis, edge-touching objects and objects smaller than 0.001 μm were removed from the counts and the Otsu threshold was applied. Independently on the method of measurement, the resulting data are given in the manuscript as long-axis length *L*.

https://doi.org/10.1021/acs.biomac.1c00501
Biomacromolecules 2021, 22, 3431−3439

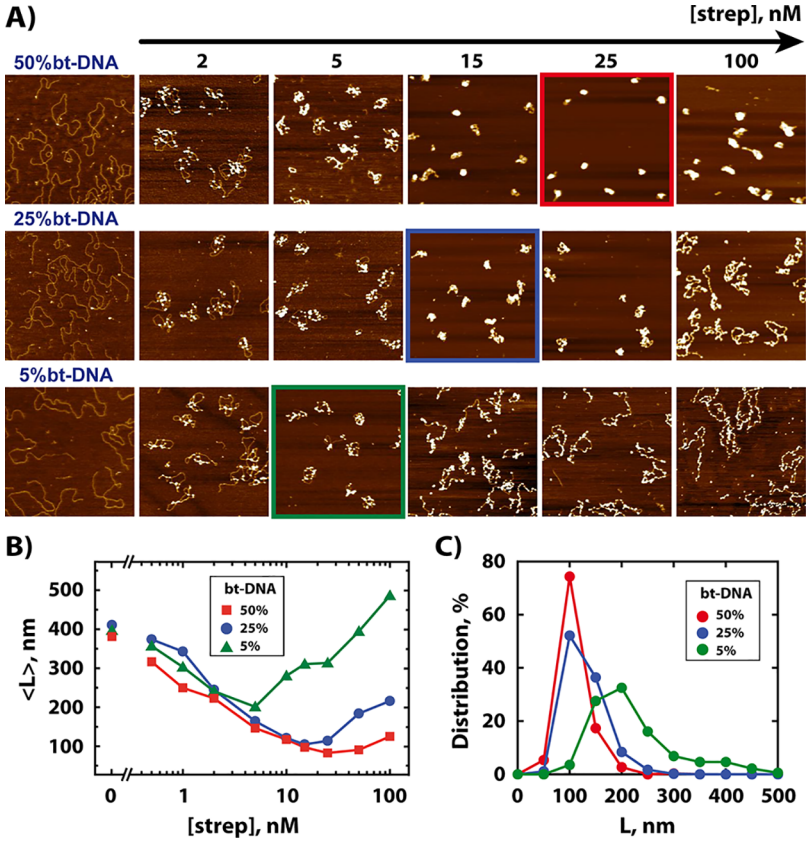

Figure 2. Effect of biotinylation density of bt-DNA on the size and morphology of DNA-streptavidin nanogels. (A) AFM observation of different bt-DNA (50%bt-DNA, 25%bt-DNA, and 5%bt-DNA) in the presence of increasing streptavidin concentrations. Images contoured with color squares indicate the streptavidin concentration at which the most compact structures were formed. All AFM images are 1 × 1 μm^2 in size. The heigth scale is adjusted for each image. (B) Size evolution of DNA-streptavidin nanogels as function of [strep] determined as the mean long-axis length $\langle L \rangle$ of the observed structures. (C) Distributions of the long-axis lengths L for the most compact nanogels corresponding to the contoured images in panel (A). [bt-DNA] = 1 μM in phosphate groups.

3. RESULTS AND DISCUSSION

To establish multiple intramolecular cross-links within multi-biotinylated DNA (bt-DNA), we exploited streptavidin-biotin binding that is considered to be the strongest known non-covalent interaction with the binding constant K_a = 2.5 × 10^{13} M^{-1}.[29] Preparation of the bt-DNA backbone is schematically described in Figure 1A. Double-stranded DNA fragments (3480 bp) were first amplified from a plasmid DNA by polymerase chain reaction (PCR) in the presence of synthetic biotinylated deoxycytidine triphosphate nucleotide (bt-dCTP) having the biotin moiety bound with a 16-atom linker to the C5 position of cytidine. Different amounts of the bt-dCTP were used in PCR (%bt-dCTP = [bt-dCTP]/([bt-dCTP] + [dCTP]) = 50, 25, 5, and 0%) to obtain bt-DNA of controlled biotinylation rates. In addition, 5′-biotinylated PCR primers were used to ensure the presence of biotin residues at each extremity of the resulting biotinylated DNA to avoid the prominence of free DNA ends from nanogel particles. The successful incorporation of the bt-dCTP into the DNA amplicons was first assessed by observing a decrease in migration in agarose gel electrophoresis of the bt-DNA compared to the non-biotinylated DNA (Figure S1).[30,31] The amplified DNA fragments were then purified by extraction of the corresponding bands from agarose gel, and their biotinylation rates were analyzed by the fluorescence biotin quantitation assay after DNA digestion with nuclease.[32] This digestion step ensured the detection of the totality of individual biotin residues by avoiding possible interferences due to both steric and electrostatic effects of the DNA duplex (Figure S2). The biotinylation efficiency in amplified DNA was measured for different ratios of biotinylated dCTP (%bt-dCTP) in the PCR mix (Figure 1B). For simplicity, the resulting bt-DNAs were named according to the %bt-dCTP used for their preparation: 50%bt-DNA, 25%bt-DNA, and 5% bt-DNA correspond to the bt-DNA obtained in the presence of 50, 25, and 5% of bt-dCTP, respectively. Figure 1B demonstrates that using a higher %bt-dCTP led to more efficient DNA biotinylation. At maximum incorporation, the resulting 50%bt-DNA had in average one biotin for every nine base pairs. DNA is a semi-flexible polylectrolyte with a monomer size of around 0.34 nm and a persistence length of 50 nm, thus ensuring a local stiffness at a distance larger than the inter-biotin distance. By assuming a random incorporation of biotin during PCR, this density corresponds to an average distance of around 3 nm between two consecutive biotins. This value is comparable with the size of streptavidin protein itself having a radius of gyration of ∼2.2 nm and the maximum length considering all its orientations of ∼6.5 nm.[33] For 25% bt-DNA and 5%bt-DNA, the measured biotinylation efficiency corresponds to the average distance between two biotins along the DNA of 10 and 30 nm, respectively.

We then investigated the morphology of the structures formed by bt-DNA of different biotinylation densities in the presence of increasing streptavidin concentrations [strep]

https://doi.org/10.1021/acs.biomac.1c00501
Biomacromolecules 2021, 22, 3431−3439

(Figures 1C and 2). The experiments were performed as follows. Streptavidin was added to fixed concentrations (1 μM in phosphate groups) of 50%bt-DNA, 25%bt-DNA, or 5%bt-DNA in 10 mM Tris/HCl buffer (pH 7.4) at 0 °C followed by immediate mixing of the samples. After 1 h of incubation on ice, the samples were adsorbed on the surface of the spermine-treated mica substrate, rinsed, dried, and then observed by atomic force microscopy (AFM). The corresponding AFM images are shown in Figure 2A and Figures S3−S5. In the absence of streptavidin, all the bt-DNA appear as long, stretched out polymer coils having a rather homogeneous height of 0.34 ± 0.08 nm, in agreement with previous measurements of dried double-stranded DNA on the mica substrate.[34−37] Addition of small amounts of streptavidin induced the appearance of clearly distinguishable streptavidin cross-linking points (see the [strep] = 1 nM condition in Figure S5) with a typical height of 2.1 ± 0.4 nm.[36] Upon the increase in [strep], two regimes could be observed. In the first one, the number of observed streptavidin per chain increased, which was accompanied by a compaction of the structures. Meanwhile, in the second one, the amount of bound streptavidin continued to increase but the structures extended again, demonstrating the saturation of the biotin residues with streptavidin molecules. AFM enabled us to measure the long-axis length (L) of the observed structures defined as their maximal Feret diameter. While length distributions were broad (Figure S6), the evolution of the average values $\langle L \rangle$ with increasing [strep] could be extracted (Figure 2B and Table S2). Upon increasing [strep], for all three biotinylation conditions, a progressive compaction of bt-DNA was observed until the most compact state was reached, after which any further addition of streptavidin led to the larger nanogel structures. We could thus define an optimal streptavidin concentration [strep]* at which the nanogels had the smallest apparent size. For 5%bt-DNA, 25%bt-DNA, and 50%bt-DNA, the [strep]* values were found at 5, 15, and 25 nM, respectively. For all bt-DNA, this corresponded to similar biotin-to-streptavidin ratios ranging between 1:1 and 1:2, which indicated that the system was controlled by strong and almost quantitative biotin-streptavidin binding. For instance, for 50%bt-DNA, if one assumed that all streptavidin molecules were binding to DNA, then this condition corresponded to ∼170 streptavidins per one DNA molecule. The average size of the NG at [strep]* also depended on the DNA biotinylation density (Figure 2B,C and Figure S6). For 5%bt-DNA, the size distribution at [strep]* was rather broad (Figure S6C) with the average long-axis length $\langle L \rangle$ = 201 ± 91 nm. The size distributions were sharper for both 25%bt-DNA and 50%bt-DNA (Figure S6A,B), and the corresponding $\langle L \rangle$ values were found to be 105 ± 33 and 83 ± 28 nm, respectively, showing that a higher number of cross-links could be formed within bt-DNA of stronger biotinylation rates. Finally, AFM enabled to characterize the height of the adsorbed objects. NGs observed for 50%bt-DNA at [strep]* corresponded to the objects of higher topography (Figure S7) and thus represented less deformable structures upon adsorption and drying. In particular, the maximum heights of the NGs formed from 50%bt-DNA, 25%bt-DNA, and 5%bt-DNA at [strep]* were found to be 13.1 ± 3.0, 6.8 ± 1.7, and 2.9 ± 0.4 nm, respectively, when imaged on a dried substrate.

Thermal and temporal stabilities were then assessed for the NGs formed from 50%bt-DNA at [strep] = 50 nM. We found that the NGs kept their structure up to temperatures of 70−80 °C (Figure S8), but they were prone to aggregate when simply kept at 4 °C in less than 2 days (Figure S9A,B). However, much more stable structures were obtained in the presence of higher streptavidin concentration ([strep] = 100 nM). In these conditions, even after 1 month of incubation at 4 °C, the NGs did not aggregate and only slightly loosened their structure (Figure S9C,D). These results can be explained by the presence of both streptavidin molecules and available biotin moieties on the surface of the NGs at [strep] close to the [strep]*, thus making the inter-NG streptavidin-biotin binding possible. A further increase in [strep] led to the saturation of all biotin residues and hindered such binding. By zetametry analysis, we found that the ζ-potential of 50%bt-DNA did not vary upon addition of streptavidin (Figure S10). Because streptavidin did not affect the charge of DNA, the nanogels remained negatively charged upon compaction of the bt-DNA. As a consequence, despite their small size, this conferred them strong colloidal stability in the conditions where streptavidin-biotin interactions between the nanogel particles were strongly limited (e.g., with excess streptavidin).

An advantage of streptavidin-induced DNA cross-linking lies in the possibility to incorporate any chemical or biological entity conjugated to streptavidin directly during the preparation of the nanogels. We thus applied this approach for functionalization of the DNA NGs with enzymes. First, streptavidin conjugated with alkaline phosphatase (sAP) or horseradish peroxidase (sHRP) enzymes was mixed with 50%bt-DNA and incubated on ice for 2 h to enable the formation of the nanogels. We used smaller concentrations of 10 nM for sAP and sHRP compared to the [strep]* for 50%bt-DNA (25 nM) to decrease the presence of enzymes unbound to DNA. In these conditions, evaluation of sAP loading efficiency by precipitating the NGs with isopropanol (Figure S11A,B) and measuring the enzymatic activity of the supernatant (Figure S11C) indicated that at least 76% of the enzyme were bound to the NGs (Figure S11D). AFM observations confirmed successful preparation of DNA-streptavidin-enzyme NGs for sAP and sHRP having 157 ± 49 and 162 ± 48 nm long-axis lengths, respectively (Figure 3A,B (left) and Figure S12). The catalytic activity of the enzymes incorporated into the nanogels was then measured after an additional 1 h incubation on ice and compared with the activities of the control samples, i.e., the enzymes in the absence of DNA (free streptavidin-enzyme conjugates) and enzymes in the presence of non-biotinylated 0%bt-DNA (Figure 3A,B, right, 0 °C condition). All enzymatic activities (EA) were then related to the activity of fresh enzymes unfrozen right before the measurements and not subjected to the incubation step, whose EA was taken to be 100%.

The results show that the enzymes remained active upon incorporation into the NGs. Compared to the EA of freshly unfrozen enzymes, the activity of sAP incorporated into the NG slightly decreased to 75% after 3 h of incubation on ice. The same decrease was observed in the corresponding control samples, showing that the properties and stability of sAP were not affected by the DNA NGs (Figure 3A, right). Interestingly, in the same conditions, an EA higher than in the control samples was observed for HRP incorporated into the NGs (Figure 3B, right). Indeed, the activity of free sHRP and sHRP in the presence of non-biotinylated 0%bt-DNA decreased down to 26 and 24%, respectively, indicating relatively rapid degradation of the enzyme even after incubation on ice, whereas when incorporated into the nanogels, sHRP

https://doi.org/10.1021/acs.biomac.1c00501
Biomacromolecules 2021, 22, 3431−3439

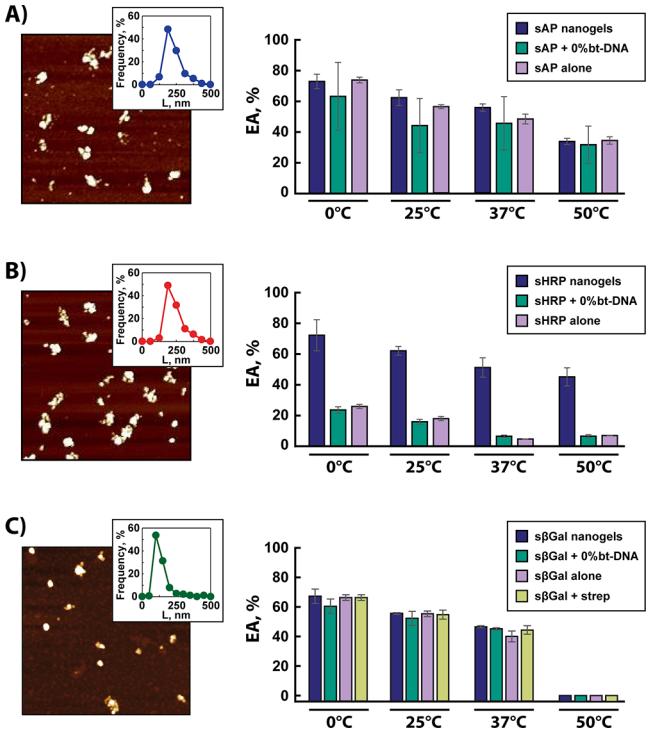

Figure 3. Enzymatic activities at different temperatures of nanogels functionalized with alkaline phosphatase (AP), horseradish peroxidase (HRP), and β-galactosidase (βGal) enzymes. Typical AFM images (left) and enzymatic activities after incubation for 1 h at different temperatures (right) for nanogels functionalized with AP (A), HRP (B), and βGal (C). The nanogels are formed from 50%bt-DNA (1 μM in phosphates) in the presence of (A) 10 nM sAP, (B) 10 nM sHRP, and (C) 1 nM sβGal and 19 nM streptavidin. The AFM images are 1.5 × 1.5 μm^2. The insets on the AFM images show the corresponding distributions of the long-axis length L of the nanogels. The activity of enzymes incorporated into the nanogels (enzyme nanogels) is compared with those in the presence of non-biotinylated DNA (enzyme + 0%bt-DNA), in the absence of DNA (enzyme alone), and for sβGal in the presence of streptavidine (sβGal + strep). For each sample, the measured EA was related to the reference EA of the corresponding freshly unfrozen enzyme whose activity was taken at 100%.

demonstrated 73% of its initial activity. The effect of DNA on the activities of conjugated enzymes has been reported in the literature, and the enhancement of the activity of enzymes by DNA conjugation has been shown for several enzymes,[18,38] especially for HRP.[20,39−43] Recently, the enhancement of the EA for HRP anchored on DNA nanostructures was explained by the local decrease in pH in close proximity to DNA compared to that in the bulk solution.[44,45] In our experiments, EA was never observed to be over 100%, so we cannot conclude on the existence of such an enhancement, but the decrease in EA was much slower for HRP incorporated into the nanogels than the enzyme alone. This could be a consequence of two effects: (i) either a weak enhancement due to the favorable local ionic microenvironment inside the DNA nanogel or (ii) stabilization of the enzyme molecules against thermal degradation, aggregation, or adsorption by incorporating them into the nanogel structure. To investigate this phenomenon, the same measurements were performed for the functionalized NGs after incubations at higher temperatures (Figure 3A,B, right). The EA of sAP gradually decreased upon incubation at higher temperatures, after 1 h of incubation at 50 °C reached 34%, and this independently on the absence or presence of the bt-DNA. Meanwhile, after incubation at 50 °C, sHRP incorporated into the NGs kept 46% of its activity, while the EA of free sHRP as well as of sHRP in the presence of 0%bt-DNA dropped down to 7%. The smaller decrease in the EA for the incorporated HRP at increased temperatures confirmed the effect of stabilization of enzymes inside the nanogels without eliminating the possibility of intrinsic enhancement inside the NG microenvironment.

HRP and AP represent examples of small and medium-size enzymes (44 and 140 kDa, respectively). We then considered the situation of a much larger protein by introducing β-galactosidase, a tetrameric enzyme of 520 kDa, into the NGs. When the streptavidin-β-galactosidase conjugate (sβGal) alone was mixed with 50%bt-DNA, the scarce structures observed by AFM had a different, less globular aspect than the previously observed nanogels (Figure S13). We thus opted for another strategy where the bulky sβGal was "diluted" with non-conjugated streptavidin during the formation of the NGs. Figure 3C (left) and Figure S14 show the successful preparation of NGs with an average long-axis length of 114 ± 58 nm. At least 95% of the used sβGal was incorporated in the gel (Figure S11E,F), and the analysis of the EA for the incorporated enzyme (Figure 3C, right) demonstrates a similar behavior to the AP enzyme. The incorporation into the DNA NGs did not affect its activity, and upon incubation at increasing temperatures, the EA of sβGal progressively decreased independently of the presence or absence of the bt-DNA.

To shed light on the smaller decrease in the EA for HRP-functionalized NGs, we investigated the effect of density of the NGs on their catalytic activity. NGs were formed either at a fixed enzyme/DNA ratio or at a fixed enzyme/biotin ratio. For this purpose, constant amounts of 50%bt-DNA, 25%bt-DNA, or 5%bt-DNA (1 μM in phosphate groups) were mixed either with a constant sHRP concentration ([sHRP] = 20 nM) or with sHRP concentration proportional to the number of biotins on the DNA (i.e., [sHRP] = 20, 13, and 2 nM for 50%bt-DNA, 25%bt-DNA, and 5%bt-DNA, respectively).

AFM observation of the resulting structures (Figure 4A and Figure S15) and the corresponding box plot distributions of the long-axis length L (Figure 4B) demonstrate different apparent sizes of the nanogels formed in these conditions. For the fixed enzyme/DNA ratio ([sHRP] = 20 nM), increasing the DNA biotinylation rate led to the formation of smaller NGs, whereas the decrease in [sHRP] in proportion to the biotin density on the bt-DNA led to the loosening of the NG structure and increase in their $\langle L \rangle$. The EA of HRP was then measured in the NGs formed in the different conditions (Figure 4C). Figure 4D shows the enzymatic activity plotted as function of the average long-axis lengths of sHRP-functionalized NGs. Independently of the conditions (fixed enzyme/DNA or enzyme/biotin ratio), all the points followed the same trend demonstrating clear correlation between the %EA of sHRP and the size of the functionalized NGs. Any detectable enhancement of the EA was observed even when the DNA-to-enzyme ratio increased by a factor of 10 ([sHRP] = 2 nM condition). In this case, the local density of DNA was probably too small to enable efficient concentration of H^+ and other cations in the proximity of the enzyme. It is thus not the amount of DNA present in the NG per enzyme but the physical density of the NGs that is responsible for the smaller decrease in the EA of the incorporated HRP upon incubation.

https://doi.org/10.1021/acs.biomac.1c00501
Biomacromolecules 2021, 22, 3431−3439

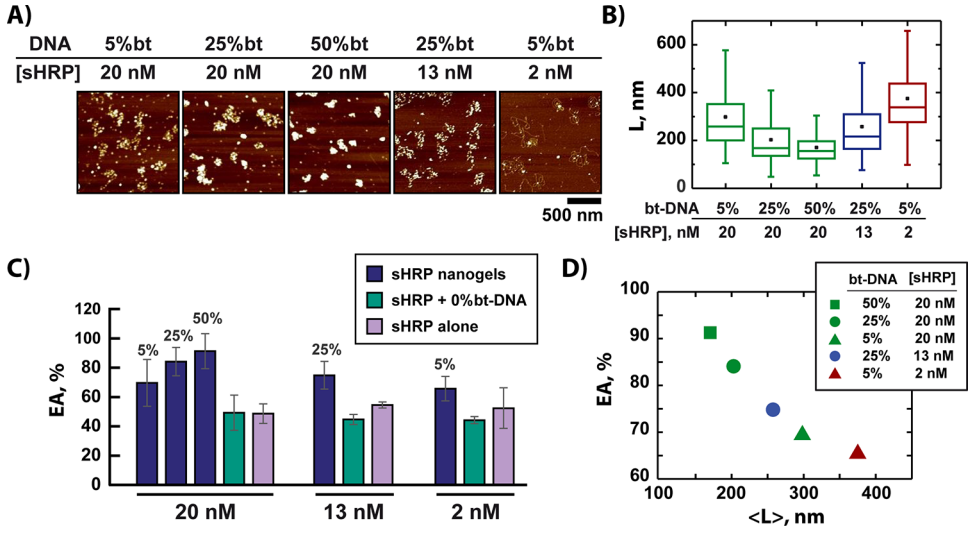

Figure 4. Effect of density of DNA nanogels on the enzymatic activity of HRP. (A) AFM images and (B) corresponding box plot distribution of the long-axis lengths L for sHRP-functionalized DNA nanogels formed from 5%bt-DNA, 25%bt-DNA, or 50%-btDNA (1 μM in phosphate groups) in the presence of 20, 13, or 2 nM sHRP. The box is determined by the 25th and 75th percentiles of the L values. Horizontal lines and squared dots in the box correspond to the median and average values, respectively, and the whiskers are determined by the 5th and 95th percentiles. (C) Comparison of the enzymatic activities of sHRP incorporated into the corresponding nanogels with the activities of sHRP alone and of sHRP in the presence of non-biotinylated 0%bt-DNA. (D) sHRP enzymatic activity as function of the average long-axis lengths of the corresponding nanogels.

This observation corroborates with the idea of a more favorable local ionic composition (particularly of the pH) inside denser DNA nanostructures.[44]

Finally, due to the presence of a large number of protein cross-links inside each nanogel particle, we explored the possibility to obtain multienzymatic nanoreactors by introducing not one but several types of enzyme-streptavidin conjugates (Figure 5A). A mixture of independent enzymes (sAP, sHRP, and sβGal) of a 20 nM final molar concentration (9.5, 9.5, and 1 nM, respectively) was added to a solution of

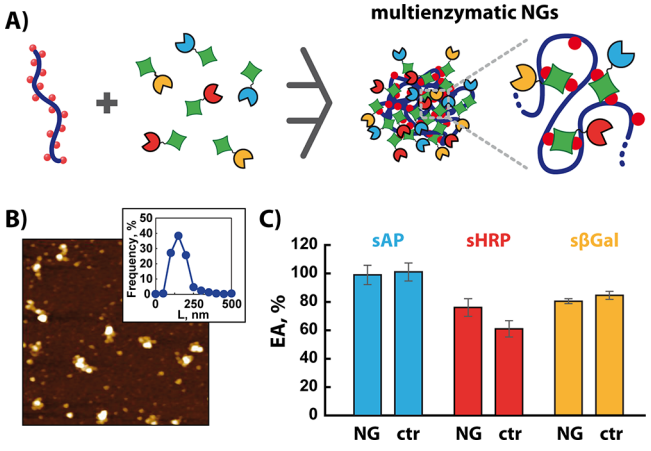

Figure 5. Preparation and catalytic activities of multienzymatic AP-HRP-βGal nanogels. (A) Scheme of preparation of multienzymatic nanogels based on simultaneous mixing of three streptavidin-enzyme conjugates with bt-DNA. (B) Typical AFM image and corresponding distribution of the long axis length L of nanogels formed from 50%bt-DNA (1 μM in phosphates) in the presence of sAP (9.5 nM), sHRP (9.5 nM), and sβGal (1 nM) conjugates. The AFM image is 1.5 × 1.5 μm^2. (C) Activities (EA) of each enzyme in the multyenzyme NGs after incubation for 1 h at 0 °C. The activity of enzymes incorporated into the nanogel (NG) is compared with those of a mixture of sAP, sHRP, and sβGal in the absence of DNA (ctr).

50%bt-DNA in the usual conditions. AFM observations of the resulting sample (Figure 5B and Figure S16) confirmed successful preparation of structures having average long-axis length $\langle L \rangle = 137 \pm 56$ nm. The activities of the three enzymes after 1 h of incubation at 0 °C were then assessed by adding corresponding substrates in separate measurements. To keep the buffer compositions constant, in the control experiment, the EA values were measured in a mixture of sAP, sHRP, and sβGal (9.5, 9.5, and 1 nM, respectively) and all the EA values were related to the EA of a mixture of freshly unfrozen enzymes. The results given in Figure 5C show that all enzymes kept their activities in the multienzymatic NGs. Moreover, the EA of the incorporated enzymes demonstrated similarities with the corresponding monoenzymatic NGs (Figure 3). Both AP and βGal kept their activities unchanged, whereas the loosening of the EA of the incorporated sHRP upon incubation was again smaller than free sHRP. All these observations thus confirm successful preparation of catalytically active multienzymatic nanoreactors based on the strongly cross-linked DNA nanogel scaffold. This approach was finally used to implement coupled enzymes (glucose oxidase (GOx) andHRP) into the DNA NGs (Figure S17). Upon oxidation of glucose by GOx, hydrogen peroxide was formed *in situ* and then used by HRP to oxidize its substrate.[45−49] Successful incorporation of both enzymes into the NGs was demonstrated by AFM (Figure S17A,B), and measurements of the enzymatic activity of HRP upon addition of glucose demonstrated that, in the used conditions, the GOx-HRP cascade kept its efficiency unchanged within the NGs (Figure S17C).

Overall, due to the high efficiency of DNA biotinylation by PCR, dense DNA nanogel particles could be obtained containing ∼100 cross-linking streptavidin molecules. By using a mixture of streptavidin-enzyme conjugates, we demonstrated successful multifunctionalization of these nanogels with different enzymes that could work independently or coupled to each other. Finally, the presence of a high number of streptavidin cross-links can enable the introduction of a larger number of different functions into the nanogels to give

https://doi.org/10.1021/acs.biomac.1c00501
Biomacromolecules 2021, 22, 3431−3439

not only complex multienzymatic systems but also nanogels carrying other functional entities, such as antibodies, aptamers, quantum dots, or magnetic nanoparticles.

4. CONCLUSIONS

In conclusion, we developed a new method for preparation of ∼100 nm DNA nanogels based on the streptavidin-biotin interaction as a source of cross-linking. Due to the possibility to easily control both the biotinylation rate of DNA by PCR and the biotin/streptavidin ratio during the nanogel preparation, the nanogels with tunable sizes and cross-linking densities could be obtained. Here, we used DNA of a fixed length decorated with a controllable number of biotin residues. PCR, however, enables straightforward control of the length of the amplified DNA, which can give access to the nanogels of fixed cross-linking density but with controllable size. Due to the protein-based cross-linking approach, the resulting DNA-streptavidin nanogels were shown to be easily functionalizable with enzymes. Monoenzymatic and multienzymatic nanogels have thus been obtained, and the catalytic activities of the incorporated enzymes were found either to be kept unchanged (alkaline phosphatase, β-galactosidase, and HRP-GOx cascade) or to be improved by the nanogel microenvironment (horseradish peroxidase), offering a protection against degradation (horseradish peroxidase). These biocompatible enzymatic nanoreactors thus constitute a novel platform for preparation of complex multifunctional systems and pave the way toward storage, transportation, and transfection into the cells of a large number of active enzymes within nanometric gel particles.

ASSOCIATED CONTENT

Supporting Information

The Supporting Information is available free of charge at https://pubs.acs.org/doi/10.1021/acs.biomac.1c00501.

Supplementary experimental methods, sequence of bt-DNA, agarose gel electrophoresis of the bt-DNAs (Figure S1), effect of DNA digestion on the measurement of DNA biotinylation (Figure S2), large-scale AFM images for DNA-streptavidin nanogels at different [strep] (Figures S3−S5), distribution of DNA-streptavidin nanogel long-axis lengths (Figure S6), 3D height profiles of DNA-streptavidin nanogels (Figure S7), thermal stability of DNA-streptavidin nanogels (Figure S8), aggregational stability of DNA-streptavidin nanogels (Figure S9), zetametric analysis of DNA-streptavidin nanogels (Figure S10), evaluation of enzyme loading efficiency into the NGs (Figure S11), large-scale AFM images of nanogels functionalized with AP and HRP enzymes (Figure S12), AFM observation of samples obtained upon mixing of 50%bt-DNA with pure sβGal (Figure S13), large-scale AFM image of nanogels functionalized with sβGal "diluted" with streptavidin (Figure S14), large-scale AFM images for sHRP-functionalized DNA nanogels of different densities (Figure S15), large-scale AFM image of multienzymatic nanogels (Figure S16), functionalization of the nanogels with GOx-HRP enzymatic cascade (Figure S17), conditions for sample preparation for AFM (Table S1), and statistical data for NG size distribution (Table S2) (PDF)

AUTHOR INFORMATION

Corresponding Author

Sergii Rudiuk − *PASTEUR, Department of Chemistry, PSL University, Sorbonne Université, CNRS, Ecole Normale Supérieure, Paris 75005, France;* orcid.org/0000-0003-1728-1163; Phone: +33 1 44 32 24 52; Email: sergii.rudiuk@ens.psl.eu

Authors

Marina Mariconti − *PASTEUR, Department of Chemistry, PSL University, Sorbonne Université, CNRS, Ecole Normale Supérieure, Paris 75005, France*

Mathieu Morel − *PASTEUR, Department of Chemistry, PSL University, Sorbonne Université, CNRS, Ecole Normale Supérieure, Paris 75005, France;* orcid.org/0000-0002-6284-1708

Damien Baigl − *PASTEUR, Department of Chemistry, PSL University, Sorbonne Université, CNRS, Ecole Normale Supérieure, Paris 75005, France;* orcid.org/0000-0003-1772-3080

Complete contact information is available at: https://pubs.acs.org/10.1021/acs.biomac.1c00501

Notes

The authors declare no competing financial interest.

ACKNOWLEDGMENTS

This work was supported by Agence Nationale de la Recherche (ANR) grants ANR-18-CE07-0001 and ANR-18-CE06-0019 and performed in part in the technology platform of the Institut Pierre-Gilles de Gennes (IPGG) with support from "Investissements d'Avenir" for Labex and Equipex IPGG (ANR-10-LABX-31 and ANR-10-IDEX-0001-02-PSL). We thank Jacques Fattaccioli for giving access to the Zetasizer apparatus and Céline Hoffmann with Virginie Escriou for fruitful discussions.

REFERENCES

(1) Seeman, N. C. DNA in a Material World. *Nature* **2003**, *421*, 427−431.

(2) Saccà, B.; Niemeyer, C. M. Functionalization of DNA Nanostructures with Proteins. *Chem. Soc. Rev.* **2011**, *40*, 5910−5921.

(3) Roh, Y. H.; Ruiz, R. C. H.; Peng, S.; Lee, J. B.; Luo, D. Engineering DNA-Based Functional Materials. *Chem. Soc. Rev.* **2011**, *40*, 5730−5744.

(4) Yan, H.; Park, S.; Finkelstein, G.; Reif, J.; LaBean, T. DNA-Templated Self-Assembly of Protein Arrays and Highly Conductive Nanowires. *Science* **2003**, *301*, 1882−1884.

(5) Rothemund, P. W. K. Folding DNA to Create Nanoscale Shapes and Patterns. *Nature* **2006**, *440*, 297−302.

(6) Hong, F.; Zhang, F.; Liu, Y.; Yan, H. DNA Origami: Scaffolds for Creating Higher Order Structures. *Chem. Rev.* **2017**, *117*, 12584−12640.

(7) Wei, B.; Dai, M.; Yin, P. Complex Shapes Self-Assembled from Single-Stranded DNA Tiles. *Nature* **2012**, *485*, 623−626.

(8) Ke, Y.; Ong, L. L.; Shih, W. M.; Yin, P. Three-Dimensional Structures Self-Assembled from DNA Bricks. *Science* **2012**, *338*, 1177−1183.

(9) Li, F.; Tang, J.; Geng, J.; Luo, D.; Yang, D. Polymeric DNA Hydrogel: Design, Synthesis and Applications. *Prog. Polym. Sci.* **2019**, *98*, 101163.

(10) Park, N.; Um, S. H.; Funabashi, H.; Xu, J.; Luo, D. A Cell-Free Protein-Producing Gel. *Nat. Mater.* **2009**, *8*, 432−437.

(11) Suhail, M.; Rosenholm, J. M.; Minhas, M. U.; Badshah, S. F.; Naeem, A.; Khan, K. U.; Fahad, M. Nanogels as Drug-Delivery

Systems: A Comprehensive Overview. *Ther. Delivery* **2019**, *10*, 697−717.
(12) Soni, K. S.; Desale, S. S.; Bronich, T. K. Nanogels: An Overview of Properties, Biomedical Applications and Obstacles to Clinical Translation. *J. Controlled Release* **2016**, *240*, 109−126.
(13) Zhang, W.; Tung, C.-H. Sequence-Independent DNA Nanogel as a Potential Drug Carrier. *Macromol. Rapid Commun.* **2017**, *38*, 1700366.
(14) Ding, F.; Mou, Q.; Ma, Y.; Pan, G.; Guo, Y.; Tong, G.; Choi, C. H. J.; Zhu, X.; Zhang, C. A Crosslinked Nucleic Acid Nanogel for Effective SiRNA Delivery and Antitumor Therapy. *Angew. Chem., Int. Ed.* **2018**, *57*, 3064−3068.
(15) Ding, F.; Huang, X.; Gao, X.; Xie, M.; Pan, G.; Li, Q.; Song, J.; Zhu, X.; Zhang, C. A Non-Cationic Nucleic Acid Nanogel for the Delivery of the CRISPR/Cas9 Gene Editing Tool. *Nanoscale* **2019**, *11*, 17211−17215.
(16) Iwasaki, Y.; Kondo, J. I.; Kuzuya, A.; Moriyama, R. Crosslinked Duplex DNA Nanogels That Target Specified Proteins. *Sci. Technol. Adv. Mater.* **2016**, *17*, 285−292.
(17) Pan, G.; Mou, Q.; Ma, Y.; Ding, F.; Zhang, J.; Guo, Y.; Huang, X.; Li, Q.; Zhu, X.; Zhang, C. PH-Responsive and Gemcitabine-Containing DNA Nanogel to Facilitate the Chemodrug Delivery. *ACS Appl. Mater. Interfaces* **2019**, *11*, 41082−41090.
(18) Jaekel, A.; Stegemann, P.; Saccà, B. Manipulating Enzymes Properties with DNA Nanostructures. *Molecules* **2019**, *24*, 3694.
(19) Thelu, H. V. P.; Atchimnaidu, S.; Perumal, D.; Harikrishnan, K. S.; Vijayan, S.; Varghese, R. Self-Assembly of an Aptamer-Decorated, DNA-Protein Hybrid Nanogel: A Biocompatible Nanocarrier for Targeted Cancer Therapy. *ACS Appl. Bio Mater.* **2019**, *2*, 5227−5234.
(20) Zhou, L.; Morel, M.; Rudiuk, S.; Baigl, D. Intramolecularly Protein-Crosslinked DNA Gels : New Biohybrid Nanomaterials with Controllable Size and Catalytic Activity. *Small* **2017**, *13*, 1700706.
(21) Templeton, N. S. The Polymerase Chain Reaction. History, Methods, and Applications. *Diagn. Mol. Pathol.* **1992**, *1*, 58−72.
(22) Wilhelm, J.; Pingoud, A. Real-Time Polymerase Chain Reaction. *ChemBioChem* **2003**, *4*, 1120−1128.
(23) Cao, L.; Cui, X.; Hu, J.; Li, Z.; Choi, J. R.; Yang, Q.; Lin, M.; Ying Hui, L.; Xu, F. Advances in Digital Polymerase Chain Reaction (DPCR) and Its Emerging Biomedical Applications. *Biosens. Bioelectron.* **2017**, *90*, 459−474.
(24) Niemeyer, C. M.; Adler, M.; Wacker, R. Immuno-PCR: High Sensitivity Detection of Proteins by Nucleic Acid Amplification. *Trends Biotechnol.* **2005**, *23*, 208−216.
(25) Medrano, R. F. V.; De Oliveira, C. A. Guidelines for the Tetra-Primer ARMS-PCR Technique Development. *Mol. Biotechnol.* **2014**, *56*, 599−608.
(26) Lo, Y.-M. D.; Mehal, W. Z.; Fleming, K. A. Rapid Production of Vector-Free Biotinylated Probes Using the Polymerase Chain Reaction. *Nucleic Acids Res.* **1988**, *16*, 8719−8719.
(27) Day, P. J.; Bevan, I. S.; Gurney, S. J.; Young, L. S.; Walker, M. R. Synthesis in Vitro and Application of Biotinylated DNA Probes for Human Papilloma Virus Type 16 by Utilizing the Polymerase Chain Reaction. *Biochem. J.* **1990**, *267*, 119−123.
(28) Green, N. M. Avidin. *Adv. Protein Chem.* **1975**, *29*, 85−133.
(29) Chilkoti, A.; Stayton, P. S. Molecular Origins of the Slow Streptavidin-Biotin Dissociation Kinetics. *J. Am. Chem. Soc.* **1995**, *117*, 10622−10628.
(30) Tasara, T.; Angerer, B.; Damond, M.; Winter, H.; Dörhöfer, S.; Hübscher, U.; Amacker, M. Incorporation of Reporter Molecule-Labeled Nucleotides by DNA Polymerases. II. High-Density Labeling of Natural DNA. *Nucleic Acids Res.* **2003**, *31*, 2636−2646.
(31) Paul, N.; Yee, J. PCR Incorporation of Modified DNTPs: The Substrate Properties of Biotinylated DNTPs. *BioTechniques* **2010**, *48*, 333−334.
(32) Batchelor, R. H.; Sarkez, A.; Cox, W. G.; Johnson, I. Fluorometric Assay for Quantitation of Biotin Covalently Attached to Proteins and Nucleic Acids. *BioTechniques* **2007**, *43*, 503−507.
(33) Haridasan, N.; Kannam, S. K.; Mogurampelly, S.; Sathian, S. P. Translational Mobilities of Proteins in Nanochannels: A Coarse-Grained Molecular Dynamics Study. *Phys. Rev. E* **2018**, *97*, No. 062415.
(34) Hansma, H. G.; Golan, R.; Hsieh, W.; Lollo, C. P.; Mullen-Ley, P.; Kwoh, D. DNA Condensation for Gene Therapy as Monitored by Atomic Force Microscopy. *Nucleic Acids Res.* **1998**, *26*, 2481−2487.
(35) Golan, R.; Pietrasanta, L. I.; Hsieh, W.; Hansma, H. G. DNA Toroids: Stages in Condensation. *Biochemistry* **1999**, *38*, 14069−14076.
(36) Rudiuk, S.; Venancio-Marques, A.; Hallais, G.; Baigl, D. Preparation of One- to Four-Branch Silver Nanostructures of Various Sizes by Metallization of Hybrid DNA−Protein Assemblies. *Soft Matter* **2013**, *9*, 9146−9152.
(37) Venancio-Marques, A.; Bergen, A.; Rossi-Gendron, C.; Rudiuk, S.; Baigl, D. Photosensitive Polyamines for High-Performance Photocontrol of DNA Higher-Order Structure. *ACS Nano* **2014**, *8*, 3654−3663.
(38) Rudiuk, S.; Venancio-Marques, A.; Baigl, D. Enhancement and Modulation of Enzymatic Activity through Higher-Order Structural Changes of Giant DNA-Protein Multibranch Conjugates. *Angew. Chem., Int. Ed.* **2012**, *51*, 12694−12698.
(39) Glettenberg, M.; Niemeyer, C. M. Tuning of Peroxidase Activity by Covalently Tethered DNA Oligonucleotides. *Bioconjugate Chem.* **2009**, *20*, 969−975.
(40) Lin, J.-L.; Wheeldon, I. Kinetic Enhancements in DNA−Enzyme Nanostructures Mimic the Sabatier Principle. *ACS Catal.* **2013**, *3*, 560−564.
(41) Gao, Y.; Roberts, C. C.; Zhu, J.; Lin, J.-L.; Chang, C. A.; Wheeldon, I. Tuning Enzyme Kinetics through Designed Intermolecular Interactions Far from the Active Site. *ACS Catal.* **2015**, *5*, 2149−2153.
(42) Zhao, Z.; Fu, J.; Dhakal, S.; Johnson-Buck, A.; Liu, M.; Zhang, T.; Woodbury, N. W.; Liu, Y.; Walter, N. G.; Yan, H. Nanocaged Enzymes with Enhanced Catalytic Activity and Increased Stability against Protease Digestion. *Nat. Commun.* **2016**, *7*, 10619.
(43) Yan, Y.; Li, J.; Li, W.; Wang, Y.; Song, W.; Bi, S. DNA Flower-Encapsulated Horseradish Peroxidase with Enhanced Biocatalytic Activity Synthesized by an Isothermal One-Pot Method Based on Rolling Circle Amplification. *Nanoscale* **2018**, *10*, 22456−22465.
(44) Zhang, Y.; Tsitkov, S.; Hess, H. Proximity Does Not Contribute to Activity Enhancement in the Glucose Oxidase−Horseradish Peroxidase Cascade. *Nat. Commun.* **2016**, *7*, 13982.
(45) Vázquez-González, M.; Wang, C.; Willner, I. Biocatalytic Cascades Operating on Macromolecular Scaffolds and in Confined Environments. *Nat. Catal.* **2020**, *3*, 256−273.
(46) Ellis, G. A.; Klein, W. P.; Lasarte-Aragonés, G.; Thakur, M.; Walper, S. A.; Medintz, I. L. Artificial Multienzyme Scaffolds: Pursuing in Vitro Substrate Channeling with an Overview of Current Progress. *ACS Catal.* **2019**, *9*, 10812−10869.
(47) Yue, L.; Wang, S.; Wulf, V.; Willner, I. Stiffness-Switchable DNA-Based Constitutional Dynamic Network Hydrogels for Self-Healing and Matrix-Guided Controlled Chemical Processes. *Nat. Commun.* **2019**, *10*, 4774.
(48) Chen, W. H.; Vázquez-González, M.; Zoabi, A.; Abu-Reziq, R.; Willner, I. Biocatalytic Cascades Driven by Enzymes Encapsulated in Metal−Organic Framework Nanoparticles. *Nat. Catal.* **2018**, *1*, 689−695.
(49) Nguyen, L. T.; Yang, K. L. Combisned Cross-Linked Enzyme Aggregates of Horseradish Peroxidase and Glucose Oxidase for Catalyzing Cascade Chemical Reactions. *Enzyme Microb. Technol.* **2017**, *100*, 52−59.

https://doi.org/10.1021/acs.biomac.1c00501
Biomacromolecules 2021, 22, 3431−3439